The Meteoritical Society

Meteoritics & Planetary Science 42, Nr 12, 2137–2152 (2007)
Abstract available online at http://meteoritics.org

The regolith portion of the lunar meteorite Sayh al Uhaymir 169

A. AL-KATHIRI[1, 2*], E. GNOS[1, 3], and B. A. HOFMANN[4]

[1]Institut für Geologie, Universität Bern, Baltzerstrasse 1, CH-3012 Bern, Switzerland
[2]Directorate General of Commerce and Industry, Ministry of Commerce and Industry, Salalah, Oman
[3]Muséum d'histoire naturelle de Genève, 1, route de Malagnou, CP 6434, CH-1211 Geneva 6, Switzerland
[4]Naturhistorisches Museum der Burgergemeinde Bern, Bernastrasse 15, CH-3005 Bern, Switzerland
[*]Corresponding author. E-mail: alikathiri34@hotmail.com

(Received 13 February 2006; revision accepted 25 June 2007)

Abstract–Sayh al Uhaymir (SaU) 169 is a composite lunar meteorite from Oman that consists of polymict regolith breccia (8.44 ppm Th), adhering to impact-melt breccia (IMB; 32.7 ppm Th). In this contribution we consider the regolith breccia portion of SaU 169, and demonstrate that it is composed of two generations representing two formation stages, labeled II and III. The regolith breccia also contains the following clasts: Ti-poor to Ti-rich basalts, gabbros to granulites, and incorporated regolith breccias. The average SaU 169 regolith breccia bulk composition lies within the range of Apollo 12 and 14 soil and regolith breccias, with the closest correspondence being with that of Apollo 14, but Sc contents indicate a higher portion of mare basalts. This is supported by relations between Sm-Al_2O_3, FeO-Cr_2O_3-TiO_2, Sm/Eu and Th-K_2O. The composition can best be modeled as a mixture of high-K KREEP, mare basalt and norite/troctolite, consistent with the rareness of anorthositic rocks. The largest KREEP breccia clast in the regolith is identical in its chemical composition and total REE content to the incompatible trace-element (ITE)- rich high-K KREEP rocks of the Apollo 14 landing site, pointing to a similar source. In contrast to Apollo 14 soil, SaU 169 IMB and SaU 169 KREEP breccia clast, the SaU 169 regolith is not depleted in K/Th, indicating a low contribution of high-Th IMB such as the SaU 169 main lithology in the regolith. The data presented here indicate the SaU 169 regolith breccia is from the lunar front side, and has a strong Procellarum KREEP Terrane signature.

INTRODUCTION

Sayh al Uhaymir (SaU) 169 is a light gray-green stone (70 × 43 × 40 mm) with a mass of 206.45 g that was found in Oman in January 2002 (Russell et al. 2003; Gnos et al. 2004). The rock consists of two contrasting lithologies (Fig. 1a). Approximately 87 vol% (estimates based on eight parallel tomographic sections) consists of a holocrystalline, fine-grained poikilitic polymict KREEP-rich impact-melt breccia; the other 13 vol% is a shock-lithified regolith breccia.

Although the impact-melt breccia is characterized by extremely high Th, U, K, rare earth elements (REEs), and P contents (Gnos et al. 2004), the regolith portion of SaU 169 also shows unusually high contents of potassium, REEs, and phosphorus (KREEP) for a lunar meteorite regolith breccia, e.g., Th 8.44 ppm as compared with 4.3 ppm in Calcalong Creek (Hill and Bonyton 2003), previously considered the most KREEP-rich lunar meteorite. The regolith yields complementary data to the impact-melt breccia (IMP) portion of SaU 169, enabling better constraints on the petrogenetic history of SaU 169, especially on the absolute and relative timing of impact events (Gnos et al. 2004). In this contribution, we concentrate on studying the regolith chemistry and the rock clasts within the regolith to deduce the petrogenetic history of SaU 169.

A regolith layer completely covers the underlying lunar bedrock, except perhaps on some steep slopes (e.g., Papike et al. 1991). The formation of the regolith, sometimes referred to as "impact gardening," is known to be due to the breakup of the lunar bedrock as a result of bombardment of the Moon's surface with meteorites of variable sizes, ranging from <1 mm to tens of kilometers. All lunar samples returned by the Apollo and the Luna missions were from the regolith, rendering the regolith the main source of rock information for the Moon (Papike et al. 1991). Aside from this, all remote sensing data (e.g., Clementine, 1994; Lunar Prospector 1998–99, and SMART-1 2004–06) are derived from the top of the lunar regolith to a maximum depth of 20 cm. Thus lunar meteorites are important samples that provide additional material from random locations on the lunar surface (Korotev 2005).

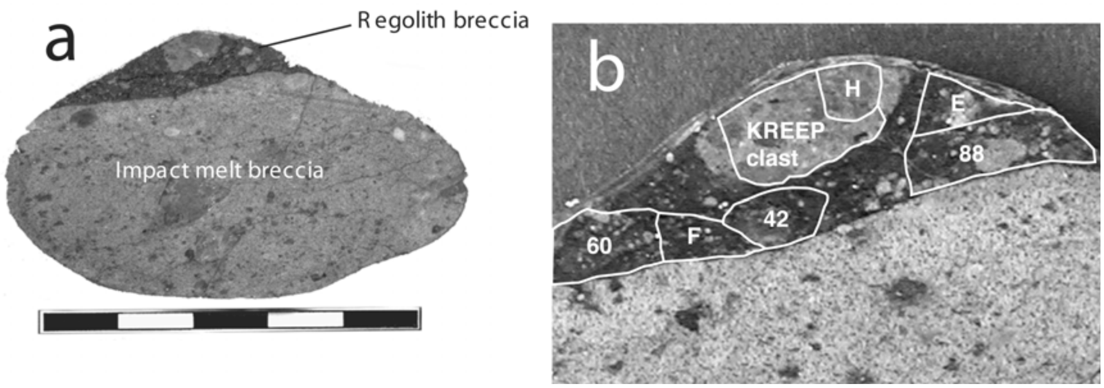

Fig. 1. Cut slice of SaU 169. a) Full slice showing the two lithologies of SaU 169: the fine-grained KREEP-rich impact-melt breccia (lower part) and the dark regolith confining a light-colored KREEP breccia clast (upper part). b) Rock slice from backside of (a) used for chemical analysis and noble gas determinations. Image width is 25 mm. Subsamples 60, 42, and 88 (mainly stage III regolith), and the large outlined part of the KREEP breccia clast (part of stage II regolith) were used for chemical analysis. Fragments H (stage II), E (mainly stage II), and F (stage III) were selected for noble gas analysis (Lorenzetti et al. 2005).

Based on the high Th content (32.7 ppm; Gnos et al. 2004) in the SaU 169 impact-melt breccia part (Fig. 1), this lithology probably comes from one of the Th hotspots as defined by Lunar Prospector γ-ray Th-maps (Lawrence et al. 1999) at the Aristarchus and Aristillus craters, the Montes Carpathus-Fra Mauro region, and the Lalande crater region. Among these Th hotspots, only areas around Lalande and southeast of the crater Aristillus are compatible with our regolith Fe-Ti-Th-K concentrations (Haskin et al. 2000; Gillis et al. 2004), based on remote sensing element distribution maps. However, the age data described by Gnos et al. (2004) of the SaU 169 render the Lalande crater area the most plausible source region for the SaU 169, since it contains craters with ages in good agreement with those obtained from SaU 169; an ~2800 Ma crater (Lalande), an ~200 Ma crater (e.g., Lalande A), and a young crater a few kilometers in size (Mösting C). It will be shown in this study that the chemistry of the average regolith, the volcanic clast types, the KREEP breccia clast, and the TiO_2 content in the basalt clasts all point to a source area in the vicinity of the Apollo 12 and 14 landing sites.

METHODS

Before cutting the meteorite, X-ray tomography was performed at the Eidgenössische Material Prüfungs Anstalt (EMPA), Dübendorf, Switzerland, to nondestructively obtain information about its interior (Fig. 1b). The industrial computer tomography (CT) scanner applied was a Scientific Measurement Systems (SMS, Austin, Texas) instrument operated at 400 kV and 2.25 mA, using linear array detectors and a detector aperture of 0.25 × 0.5 mm. Tomographs obtained had a resolution of 0.15 × 0.15 mm (pixel size).

One doubly polished thin section encompassing 1.2 cm^2 of regolith was studied by transmitted and reflected light microscopy. Mineral compositions were determined using a Cameca SX-50 or a Jeol JXA-8200 microprobe at the Institute of Geological Sciences, University of Bern, Switzerland. Beam conditions were 15 kV and 20 nA, 1–5 μm spot size, and equal measurement times on peak and background. Backscattered electron images (BSE) were obtained on the Jeol microprobe. Mineral modes were determined by point counting on BSE images.

Chemical analysis on aliquots of homogenized regolith and KREEP breccia clast were obtained by ICP-MS and ICP-OES methods at Activation Laboratories Ltd., Ancaster, Ontario, Canada. Samples were acid-dissolved after fusion with lithium metaborate/tetraborate. Errors (1σ) typically are 1–5% for main elements and 10% for traces, as estimated from rock standards used for calibration and independently measured standards. Analyses were obtained on an aliquot of 117 mg from the KREEP breccia clast and an aliquot of 185 mg from the average regolith. Sample parts used for the different methods are indicated in Fig. 1b.

RESULTS

Regoliths and Shock History

As expected in a regolith, the shock state of individual clasts varies from total melting (impact melts) to unshocked clasts. A notable and significant feature of the regolith breccia of SaU 169 is that at least two shock stages (Table 1) can be recognized, which can be dated relatively using cross-cutting relationships. Two regolith stages labeled II and III (III is younger than II, with stage I being represented by the IMB portion described in Gnos et al. 2004) can be separated. The stage II portion of the regolith, which contains the large KREEP breccia clast (Figs. 1 and 2), is characterized by a darker matrix than the stage III regolith portion, a feature that is directly related to the finer average grain size of stage II. At the contacts between the stage III regolith and the IMB and

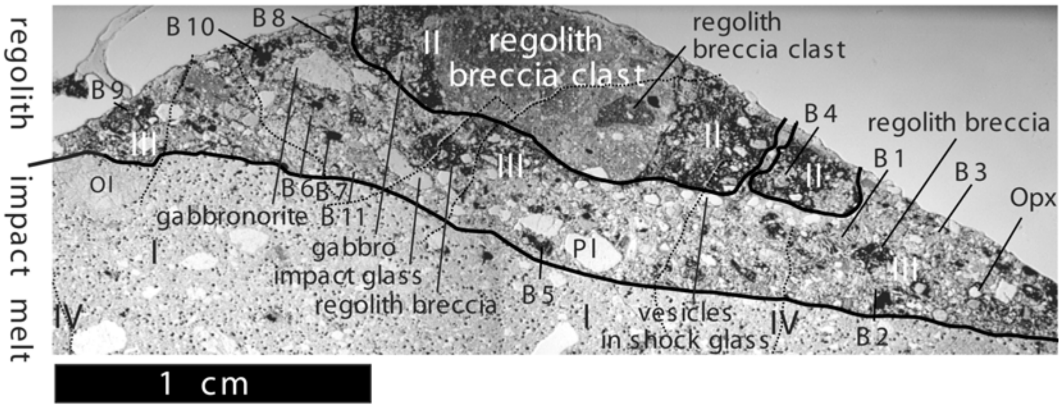

Fig. 2. Thin section overview photograph of the regolith part of the SaU 169 showing the regolith and adjacent impact-melt breccia. Marked with I to IV are clearly distinguishable stages of breccia and shock vein formation. B1–B11 mark the analyzed volcanic clasts. Ol = olivine; Pl = plagioclase; Opx = orthopyroxene. Image width is 35 mm.

Table 1. Tentative correlation of stages with events.

Stage	Lithology/evidence	Tentative age correlation
IV	Glass crosscutting I, II, III	Launch event (~0.34 Ma)
III	Breccia with glass beads, etc.	~200 Ma
II	Breccia without beads, etc.	~2800 Ma
I	IMB formation	3909 Ma

stage II and stage III regoliths, zones of impact-melt glass containing 100–600 μm-sized vesicles occur (Fig. 3). Stage III impact-melt glass also transects the older regolith material (Fig. 2), confirming the observed age relationships via laws of cross-cutting relationships.

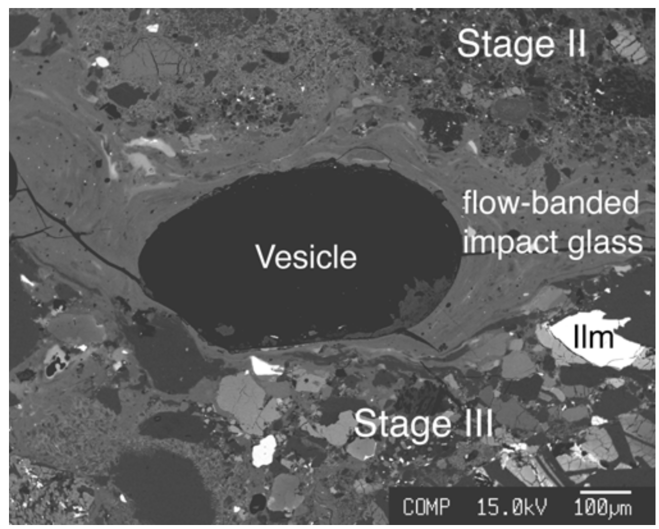

Fig. 3. BSE image 3of vesicle-rich flow-banded shock melt bordering the stage III regolith. On the image it is in contact with stage II regolith.

Regolith Clasts

Both regolith stages comprise crystalline and glassy volcanic rocks, magmatic lithic fragments, breccia fragments, fragments of mafic gabbroic rock clasts or granulites, and crystal fragments. The basaltic rock fragments reach a maximum size of ~2.0 mm × 0.9 mm (Fig. 2). The largest clast has a size of ~7.5 mm × 4 mm. It is a gray KREEP regolith breccia clast situated in the central part of regolith lithology II (Figs. 1 and 2) and contains itself fragments of regolith breccias. Yellow and orange glass fragments and glass beads occur only in regolith stage III. A set of parallel, glassy shock veins (stage IV in Fig. 2; Table 1) crosscut the two regoliths and the impact-melt breccia.

Mineralogy of Rock Clasts

The clasts, interpreted as basalt rather than impact-melt clasts, are composed of 10–500 μm-sized minerals, chiefly plagioclase laths, prismatic pyroxenes, olivine, and ilmenite. Fe-Mg silicates in the basalts generally display strong compositional zoning, and several clasts restricted to the younger regolith contain clinopyroxene with pyroxferroite rims. The classification of pyroxenes in the basalt clast is based on the nomenclature described by Morimoto et al. (1988). The mineral chemistry and the modal composition of 10 individual basalt clasts and a clast containing pyroxferroite breakdown products (clast 11) were determined (Figs. 2 and 4) and the results are compiled in Table 2. By using mineral modes and the chemical variability of the minerals, a tentative bulk compositional range for each basaltic clast was estimated. Based on the mare basalt classification suggested by Neal and Taylor (1992) and Le Bas (2001), the full range from Ti-rich (TiO_2 > 6 wt%) to Ti-poor (TiO_2 < 1.5 wt%) basalts including aluminous (Al_2O_3 > 11 wt%) members as well as picrobasalts (Le Bas 2001) seem present. In general, all analyzed basalts are low-K (K < 2000 ppm) basalts (Neal and Taylor 1992).

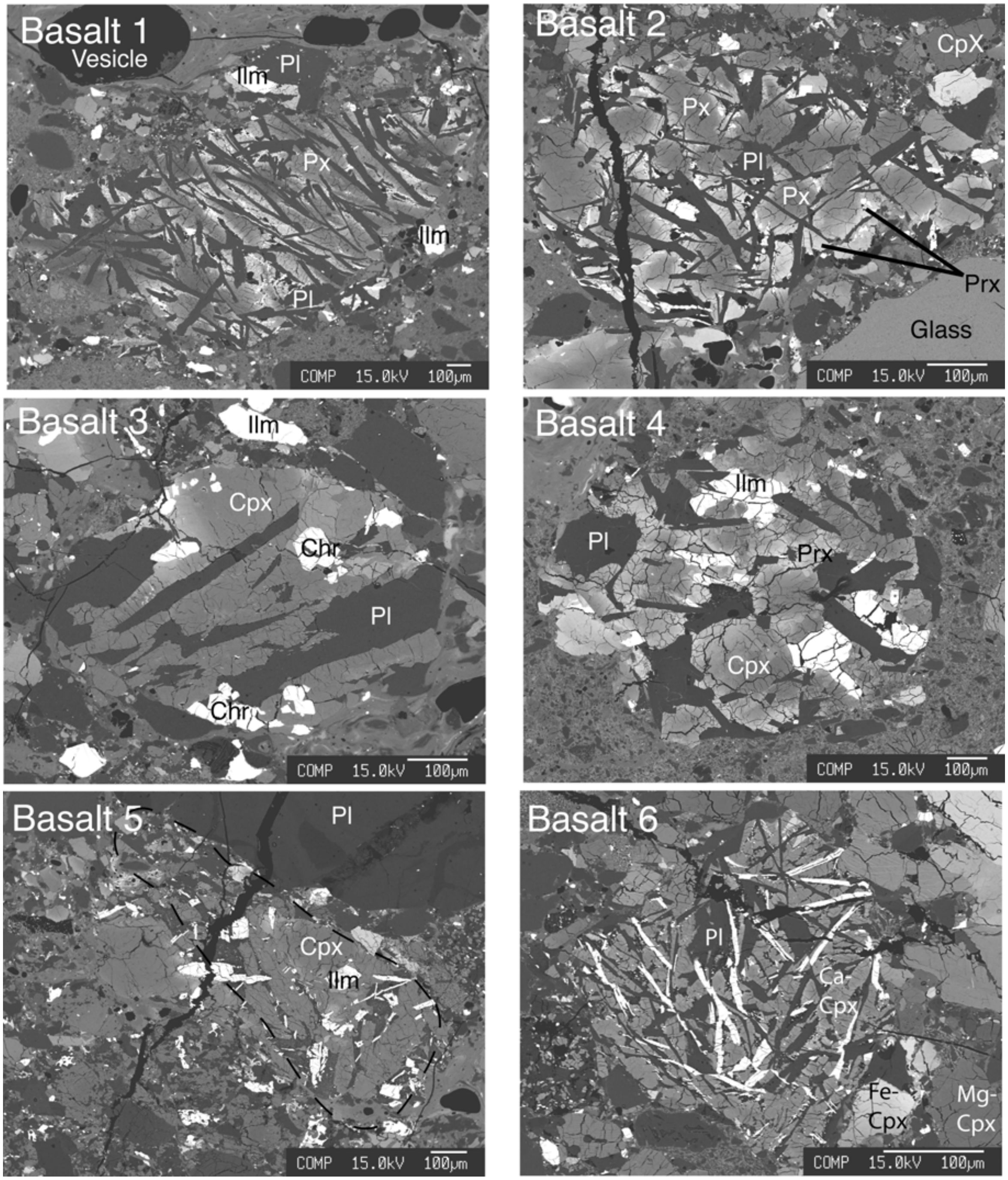

Fig. 4. BSE images of 11 basalt clasts in the younger regolith breccia (stage III). Ca-Cpx = Ca-rich clinopyroxene; Fe-Cpx = Fe-rich clinopyroxene; Mg-Cpx = Mg-rich clinopyroxene; Ilm = ilmenite; Ol = olivine; Opx = orthopyroxene; Pl = plagioclase; Prx = pyroxferroite; Chr = chromite; Fa = fayalite; Trd = tridymite. The small clast "Basalt 11" could represent a break-down assemblage after pyroxferroite.

Two Ti-rich basalts were found (basalt 5 and basalt 6; Fig. 4). Basalt 5 is an olivine picrobasalt. Basalt 6 is an aluminous Ti-rich augite basalt.

Basalt 8 is a very fine-grained olivine picrobasalt consisting of 69 vol% olivine and 24% glass (Fig. 4).

Three aluminous medium-Ti basalts (basalts 1, 7, and 10; Fig. 4) are present. Basalt 1 is a pigeonite-augite basalt containing zoned prismatic pigeonite crystals with pyroxferroite rims. Basalt 7 is an olivine-pigeonite basalt, and basalt 10 is an augite basalt.

Ti-poor basalts are more abundant, with four representatives (three of them are aluminous). Based on the model composition (Table 2), they comprise a pigeonite basalt (basalt 3), a pigeonite-augite basalt (basalt 2), and two

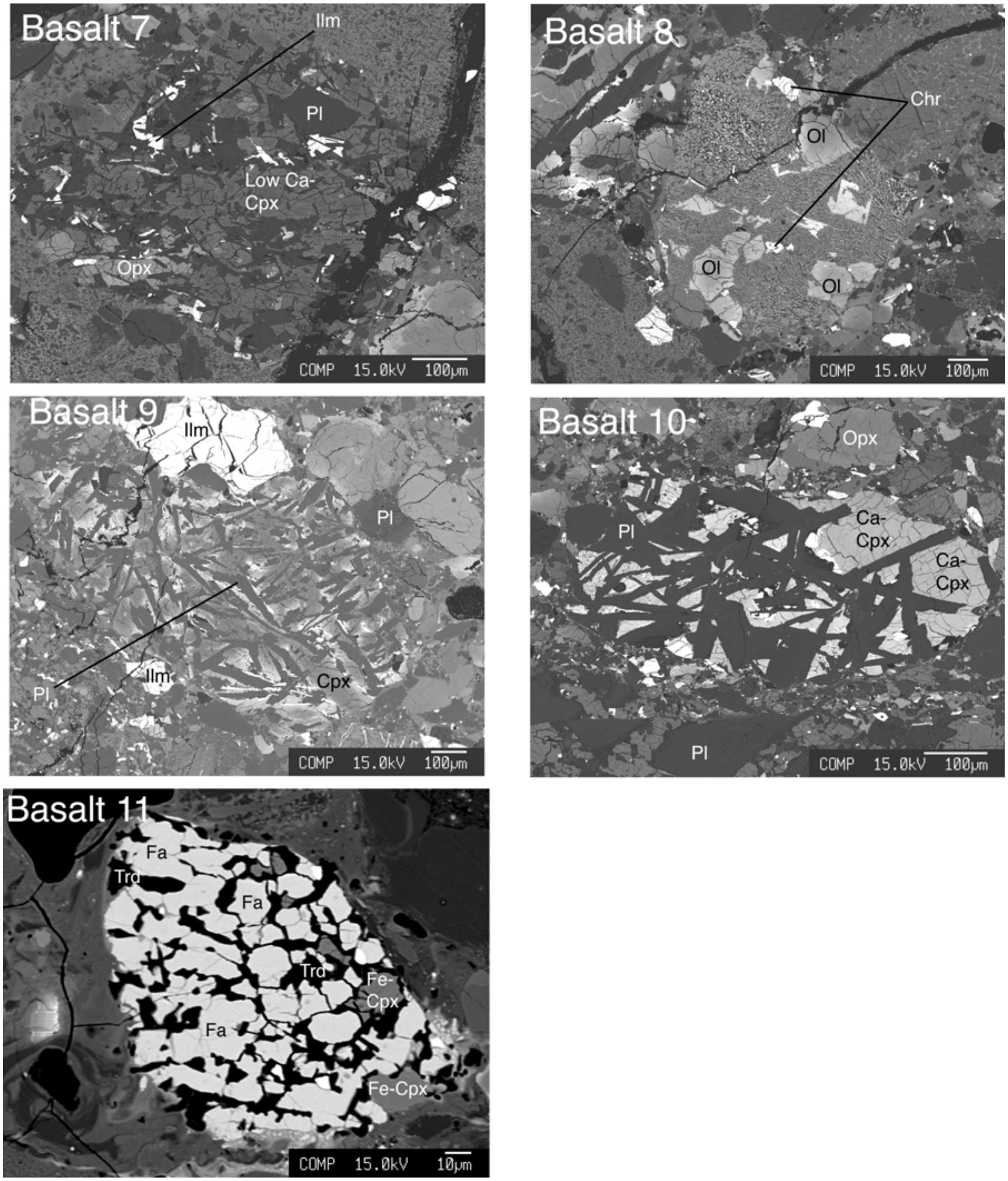

Fig. 4. *Continued.* BSE images of 11 basalt clasts in the younger regolith breccia (stage III). Ca-Cpx = Ca-rich clinopyroxene; Fe-Cpx = Fe-rich clinopyroxene; Mg-Cpx = Mg-rich clinopyroxene; Ilm = ilmenite; Ol = olivine; Opx = orthopyroxene; Pl = plagioclase; Prx = pyroxferroite; Chr = chromite; Fa = fayalite; Trd = tridymite. The small clast "Basalt 11" could represent a break-down assemblage after pyroxferroite.

augite-pigeonite basalts (basalts 4 and 9). Basalts 3 and 9 (Fig. 4) are aluminous basalts with estimated Al_2O_3 contents of 15.4 wt% and 13.9 wt%, respectively.

Basalt 11 is a clast (~140 × 160 μm) found in the regolith stage III within the flow-banded shock melt (Fig. 4). It is composed of fayalite, ferroaugite, interstitial silica, and ilmenite (Tables 2 and 3). Its bulk rock composition calculated from the mineral chemistry shows that it is Fe-rich and alkali-poor, like pyroxferroite breakdown products.

Two gabbronorite clasts are shown in Fig. 5. The larger clast (2 mm × 1.2 mm; Fig. 5a) consists of zoned pyroxene, plagioclase ($An_{96–97}Or_0$), and olivine (Fo_{61}).

The most prominent of the regolith breccia clasts is the 7.5 mm large KREEP regolith breccia clast (Figs. 1 and 2),

Table 2. Mineral and modal composition of analyzed basalts, gabbros, and breccia clasts in SaU 169 regoliths (stages II–III).

Clast (lithology; stage)	Lithology	Mineralogy	Pyx (vol%)	Ol (vol%)	Opaques (vol%)	Plg (vol%)	Glass (vol%)	Al_2O_3 (wt%)	TiO_2 (wt%)	K_2O (wt%)
Volcanic										
Basalt 1 (III)	Augite-pigeonite basalt (aluminous medium-Ti)	Zoned Px($En_{43-59}Wo_{9-23}$) Prx (En_2Wo_{13}) Pl ($An_{90}Or_{0-1}$) Ilm (Ilm_{91}) Spl($Chr_{19}Usp_{60}$)	39	–	3	58	–	~18.1	~2.8	~0.03
Basalt 2 (III)	Pigeonite-augite basalt (Ti-poor)	Px ($En_{20-52}Wo_{7-27}$ Prx (En_1Wo_{14-17} Pl ($An_{86-87}Or_{0-1}$) Spl ($Chr_{6-10}Usp_{87-82}$)	67	–	2	31	–	~9.1	~1.4	~0.08
Basalt 3 (III)	Pigeonite basalt (aluminous Ti-poor)	Px ($En_{46}Wo_{18}$) Pl ($An_{90}Or_{0-1}$) Chr ($Chr_{42-45}Usp_{10}$)	47	–	6	48	–	~15.4	~1.0	~0.03
Basalt 4 (III)	Augite-pigeonite basalt (Ti-poor)	Px ($En_{26-40}Wo_{18-31}$) Prx ($En_{13-19}Wo_{18-19}$) Pl ($An_{75-85}Or_{1-2}$) Ilm (Ilm_{98}) Spl (Chr_8Usp_{79})	68	–	1	31	–	~8.9	~1.5	~0.06
Basalt 5 (III)	Olivine basalt (Ti-rich)	Pl ($An_{65-95}Or_{1-3}$) Ol (Fo_{47-62}) Ilm (Ilm_{84-85})	–	63	11	26	–	~6.9	~8.0	~0.02
Basalt 6 (III)	Augite basalt (aluminous Ti-rich)	Px ($En_{22-32}Wo_{23-28}$) Pl ($An_{75-82}Or_{1-2}$) Ol (Fo_{61-62}) Ilm (Ilm_{87})	41	–	14	45	–	~18.6	~6.4	~0.07
Basalt 7 (III)	Olivine-pigeonite basalt (aluminous medium-Ti)	Px ($En_{65-68}Wo_7$) Pl ($An_{78-87}Or_1$) Ol (Fo_{63-64}) Ilm (Ilm_{96})	47	7	6	40	–	~11.5	~5.0	~0.04
Basalt 8 (III)	Olivine basalt, probably picrobasalt (very fine grained)	Ol (Fo_{48-55}) Chr ($Chr_{38}Usp_{26}$)	–	69	7	–	24	–	–	–
Basalt 9 (III)	Augite-pigeonite basalt (aluminous Ti-poor)	Px ($En_{38-49}Wo_{9-22}$) Prx ($En_{2-7}Wo_{9-15}$) Pl ($An_{85-91}Or_{0-1}$) Ol (Fo_{60}) Ilm (Ilm_{96})	58	1	3	39	–	~12.9	~1.3	~0.02
Basalt 10 (III)	Picrobasalt (aluminous medium-Ti)	Px ($En_{4-14}Wo_{25-34}$) Pl ($An_{73-83}Or_{1-2}$) Ilm (Ilm_{98})	48	–	3	49		~13.9	~2.9	~0.15
Basalt 11 (III)	Picrobasalt (ferrous)		6	67	1	–	26	~0.3	~0.9	~0.03
Non-volcanic										
Gabbro (III)	Gabbronorite	Px ($En_{41-48}Wo_{5-24}$) Pl ($An_{96-97}Or_0$) Ol (Fo_{61})								
Breccia (II)	KREEP breccia clast	Trd, Pl ($An_{78-97}Or_{0-1}$)								

Px = pyroxene; Prx = pyroxferroite; Ol = olivine; Pl = plagioclase; Ilm = ilmenite; Chr = chromite; Spl = spinel; Trd = tridymite.
(II) and (III) refer to regolith stages shown in Fig. 2.

Table 3. Representative microprobe analysis (wt%) of basalt 11 clast.

	Fayalite	Fayalite	Ferroaugite	Ferroaugite	Silica	Silica
SiO_2	31.53	31.75	50.35	50.57	96.17	97.69
TiO_2	0.08	0.05	0.28	0.33	0.08	0.05
Cr_2O_3	0.06	b.d.	b.d.	b.d.	b.d.	b.d.
Al_2O_3	0.02	0.04	0.43	0.50	0.25	0.97
FeO	59.30	59.23	21.98	20.38	2.50	1.09
MnO	0.88	0.85	0.37	0.34	0.04	b.d.
NiO	b.d.	0.03	b.d.	b.d.	0.03	b.d.
MgO	7.13	7.07	6.98	7.23	0.16	b.d.
CaO	0.11	0.14	19.07	20.48	0.10	0.21
Na_2O	b.d.	b.d.	0.08	0.08	b.d.	0.06
K_2O	b.d.	b.d.	b.d.	b.d.	b.d.	0.10
Total	99.11	99.16	99.54	99.91	99.33	100.17
Normalized to	4 O	4 O	6 O	6 O	4 O	4 O
Si	1.014	1.019	1.999	1.990	1.968	1.969
Ti	0.002	0.001	0.008	0.010	0.001	0.001
Cr	0.002	0.000	0.000	0.000	0.000	0.000
Al	0.001	0.002	0.020	0.023	0.006	0.023
Fe	1.595	1.590	0.730	0.671	0.043	0.018
Mn	0.024	0.023	0.013	0.011	0.001	0.000
Ni	0.000	0.001	0.000	0.000	0.000	0.000
Mg	0.342	0.338	0.413	0.424	0.005	0.000
Ca	0.004	0.005	0.811	0.864	0.002	0.004
Na	0.000	0.000	0.006	0.006	0.000	0.002
K	0.000	0.000	0.000	0.000	0.000	0.003
Mg %	17.6	17.5	21.1	21.7	–	–
Fe %	82.4	82.5	41.5	44.1	–	–
Ca %	–	–	37.4	34.2	–	–

b.d. = Below detection.

which mainly consist of a very fine-grained gray matrix enclosing larger mineral clasts of Ca-rich plagioclase ($An_{78–97}$), olivine (typically <500 μm), and a few laths or angular grains of silica. The clast further contains abundant ilmenite and hypidiomorphic zircons up to 50 μm in size. The regolith breccia clast also contains at least one breccia fragment (Fig. 2). Silica minerals and zircon occur also in other breccia clasts (Fig. 6).

Mineral Clasts

Mineral clasts in the regoliths are commonly ≤1 mm in size; only a few plagioclase clasts are >1 mm with a largest grain size of 2 mm (Fig. 2). Pyroxene and olivine clasts are <600 μm in size and ilmenites are 100–400 μm in size. Unzoned mineral clasts in the regolith breccia cover a wider compositional range than rock fragments. The plagioclase clast chemistry ranges from An_{74} to An_{94} and Or_0 to Or_2. Most olivine clasts in the regolith are Mg-rich ($Fo_{66–73}$) with one unzoned olivine clast in the stage III regolith breccia showing a composition of Fo_{84}. On the other hand, a >200 μm-sized, unzoned olivine grain of fayalitic composition (Fo_{12}) is also present in the stage III regolith breccia (Fig. 7). Pyroxene clasts include both Mg- and Fe-rich members and Ca-rich to Ca-poor clinopyroxenes. Pyroxenes displaying exsolution texture (Fig. 8) are rare. Ilmenite clasts show a wider compositional range of $Ilm_{85–96}$ than ilmenites in basalt clasts. Troilite is observed as small fragments in the regolith ground mass and as tiny inclusions in the largest glass fragment (Fig. 9a).

Glass

Only the stage III regolith breccia contains unaltered yellow and orange glass shards and beads. Glass beads range from <1 mm to a maximum size of 2 mm (Fig. 9). They are commonly elongated in shape with irregular boundaries. The largest glass fragment contains small inclusions of plagioclase, troilite, and baddeleyite (Fig. 9a). The major elements composition of glass clasts is similar to the average regolith except for one bead having higher Al_2O_3, CaO, and lower FeO content, probably due to contamination of plagioclase schlieren (Table 4). The glass beads have Mg/Al ratios of ~0.5 (Table 4), which is different from typical Mg/Al ratios of 1.7 to 3 found in lunar volcanic glass (Delano 1986).

The shock melt glass associated with the younger regolith (stage III) is composed of bands showing different gray shadings on BSE images (Fig. 3). Dark bands, gray areas

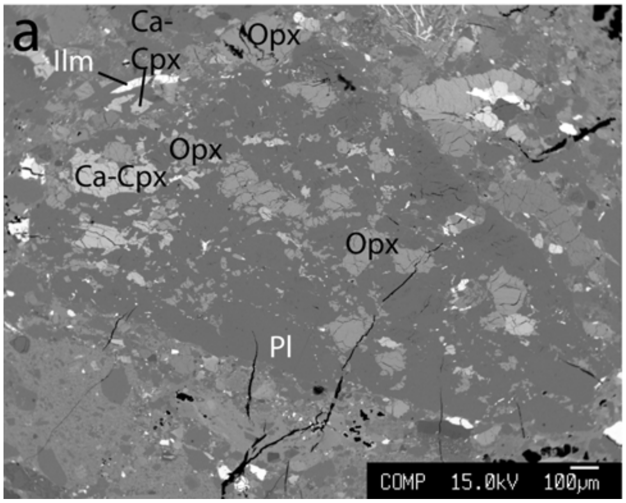

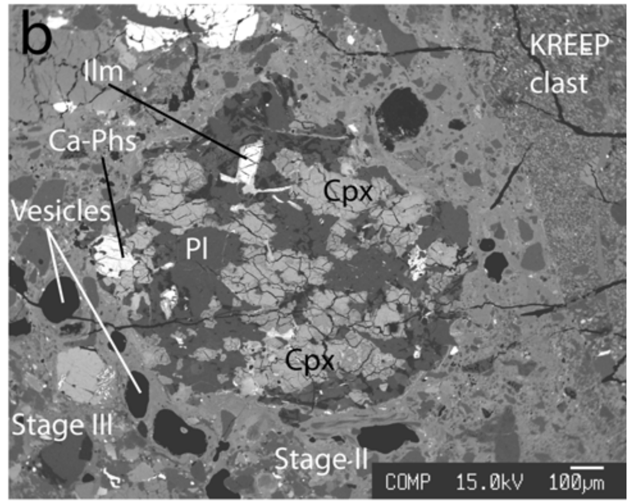

Fig. 5. The two largest fine-grained gabbroic rock fragments. a) Deformed gabbronorite and (b) gabbro consisting mainly of plagioclase (Pl), orthopyroxene (Opx), clinopyroxene (Cpx), Ca-rich clinopyroxene (Ca-Cpx), ilmenite (Ilm), and Ca-phosphate (Ca-Phs).

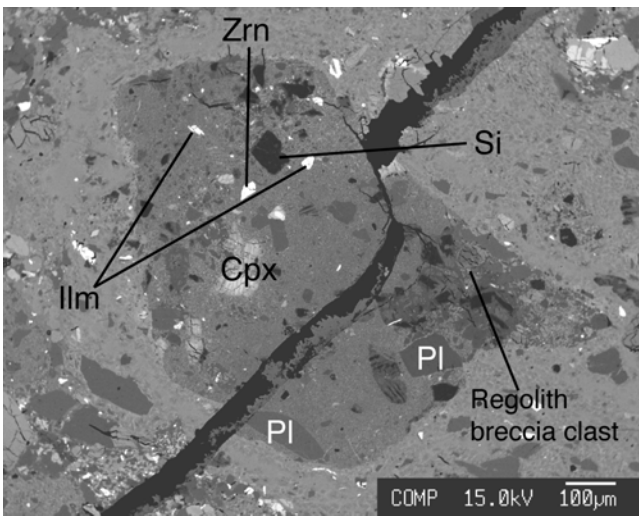

Fig. 6. Regolith breccia clast cut by crack filled with terrestrial calcite. The breccia consists mainly of a fine groundmass containing plagioclase (Pl), clinopyroxene (Cpx), and ilmenite (Ilm) fragments. An idiomorphic SiO_2-grain (Si) and a zircon clast (Zrn) are also visible.

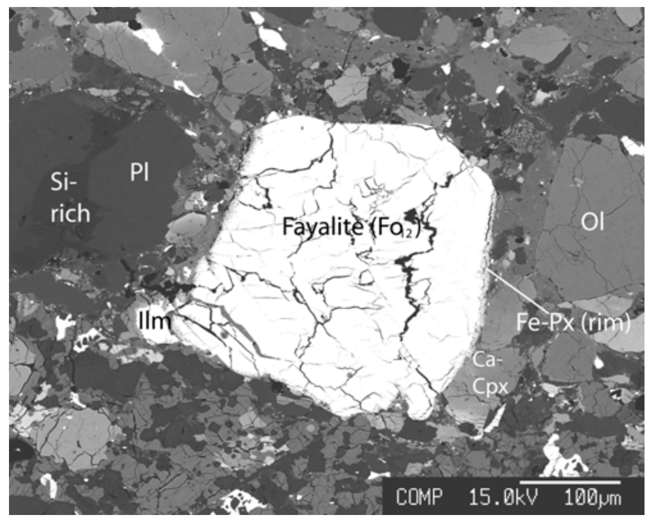

Fig. 7. Large compositionally homogenous fayalite clast (Fo_{12}). Note the thin Fe-rich pyroxene rim on the fayalite. Ol = Mg-Fe olivine; Ca-px = Ca-rich clinopyroxene; Ilm = ilmenite; Pl = plagioclase; Si-rich = SiO_2-rich melt.

and light bands can be distinguished. Microprobe analysis of these different bands showed that the dark flow bands are enriched in Al_2O_3, the gray areas have lower Al_2O_3 content and the light bands are low in Al_2O_3 but enriched in FeO (Table 4). The gray areas have Mg/Al ratios of about ~0.3, but the dark and light band have strongly variable Mg/Al ratios ranging from 0.07 to 6.00 (Table 4).

Regolith Bulk Chemistry

The bulk composition of SaU 169 regolith is presented on Table 5 together with data for the KREEP breccia clast, impact breccia main lithology, and Apollo 14 high-K KREEP. Our regolith data are consistent with data obtained by INAA at Washington University (Zeigler et al. 2006; Korotev, personal communication 2007), showing an average deviation of 16% for concentrations of 24 comparable elements.

Typical lunar Fe/Mn mineral ratios (Moon 60–80; Papike 1998; Papike et al. 2003) were obtained for the regolith (80) and the KREEP breccia clast (74), and oxygen isotopes obtained on the IMB also yielded lunar values (Gnos et al. 2004). K/U values for the average regolith (1682) and the KREEP breccia clast (1253) are also typically lunar (Moon 1700; Papike 1998; Papike et al. 2003).

A comparison of the CI chondrite-normalized (Anders and Gravesse 1989) REE concentrations of soils and regolith

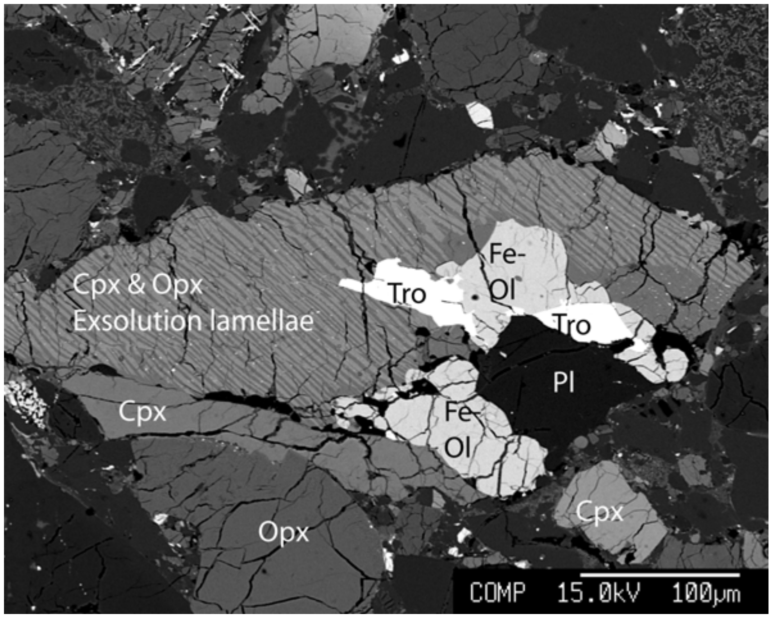

Fig. 8. Rock clast consisting mainly of Ca-pyroxene showing 1–2.5 µm wide exsolution lamellae of Mg-pyroxene (dark). It is associated with plagioclase (Pl), Mg-orthopyroxene (Opx), clinopyroxene (Cpx), Fe-rich olivine (Fe-Ol), and troilite (Tro).

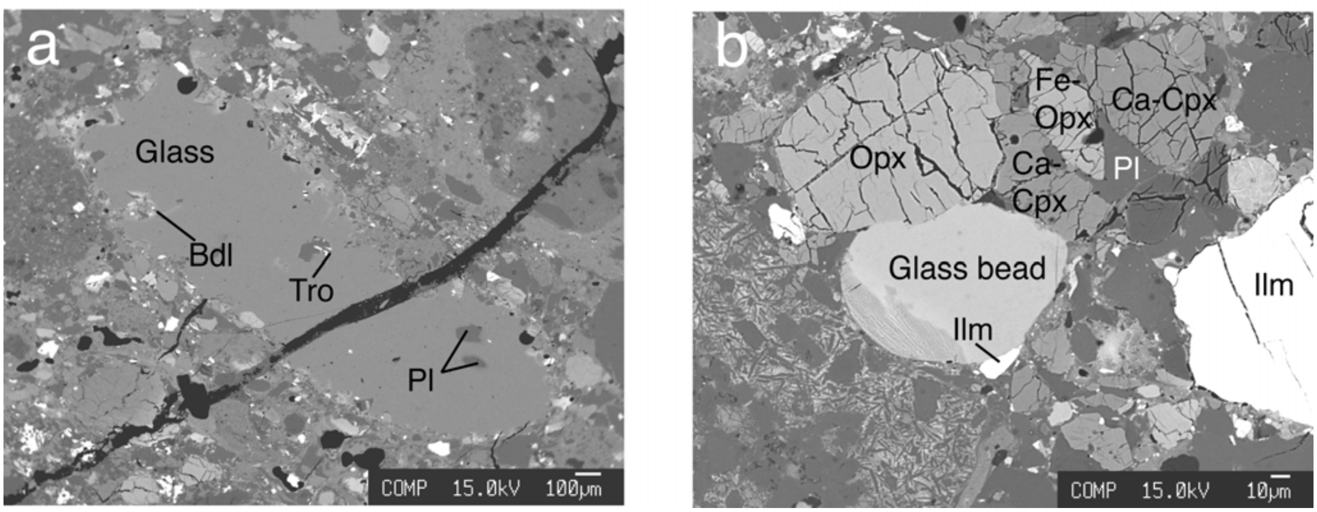

Fig. 9. Impact glass fragments. a) 2 mm-sized glass shard containing small inclusions of plagioclase (Pl), troilite (Tro), and baddeleyite (Bdl; ZrO_2). b) Small glass bead surrounded by pyroxene, plagioclase, and ilmenite. Note the quenched crystallites in the glass bead at the contact to a fine-crystalline impact-melt pocket.

breccias from Apollo 11–17 landing sites (Haskin and Warren 1991) and the Apollo 14 KREEP breccias (Warren and Wasson 1979) show that the SaU 169 bulk regolith REE content is slightly lower than for minimum soil and regolith breccias from the Apollo 14 landing site, but higher than the maximum values of Apollo 11, 12, 15, 16, and 17 soils. The SaU 169 regolith chemical composition for most elements is intermediate between Apollo 12 and 14 regoliths. The KREEP breccia clast REE content and slope is very similar to the KREEP component based on the average composition of Apollo 14 breccias.

The bulk regolith breccia and the KREEP regolith breccia clast are not depleted in alkalis based on K/U of 1680 and K/U of 1253, respectively. The SaU 169 Sc concentrations of 28 ppm in the regolith breccia and of 18 ppm in the KREEP breccia clast contained in the breccia are higher than those of the Apollo 16 regolith breccias, which are <12 ppm (Cahill et al. 2004; Korotev 1997). A plot of Sm versus Al_2O_3 (Fig. 10) shows that the regolith breccia plots in the field of the Apollo 14 regolith breccias (Cahill et al. 2004; Warren and Wasson 1980) while other lunar regoliths are less similar (Cahill et al. 2004). The SaU 169 regolith La/Yb

Table 4. Representative microprobe analysis (wt%) of glass fragments, glass beads, and banded shock melt.

	Glass fragment	Plagioclase inclusion	Glass fragment	Glass bead	Glass bead	Glass bead	Gray band	Gray band	Av. gray bands (n = 10)	Light band	Light band	Dark band	Dark band
SO_3	n.a.	n.a.	n.a.	n.a.	n.a.	n.a.	0.21	0.22	0.17(7)	0.01	0.01	0.09	0.04
P_2O_5	n.a.	n.a.	n.a.	n.a.	n.a.	n.a.	0.38	0.37	0.31(7)	0.00	0.02	0.21	0.07
SiO_2	46.97	47.82	47.09	46.86	46.8	47.02	45.63	45.83	46.13(71)	47.59	47.23	45.49	46.23
TiO_2	2.25	0.03	2.36	2.3	2.25	2.23	2.19	2.15	2.11(13)	1.05	1.12	1.34	0.45
Cr_2O_3	0.24	b.d.	0.21	0.3	0.33	0.31	0.17	0.20	0.18(6)	0.12	0.18	0.06	0.06
Al_2O_3	17.39	30.82	17.49	17.51	17.53	17.45	20.95	20.32	21.18(91)	1.23	1.88	23.39	30.12
FeO	11.62	2.56	11.29	11.28	11.25	11.21	9.81	9.54	8.78(91)	27.80	31.35	8.16	2.96
MnO	0.18	0.02	0.14	0.17	0.16	0.18	0.14	0.16	0.14(2)	0.46	0.57	0.15	0.06
NiO	b.d.	b.d.	0.03	0.04	0.02	0.04	0.00	0.05	0.01(2)	0.02	b.d.	b.d.	b.d.
MgO	8.00	1.41	7.67	7.79	7.78	7.82	5.80	6.15	5.68(48)	6.46	5.71	5.23	1.89
CaO	11.62	15.41	11.38	11.61	11.38	11.38	12.64	12.92	12.94(42)	13.30	10.68	13.51	16.80
Na_2O	0.57	1.53	0.62	0.62	0.61	0.58	0.87	0.84	0.89(7)	0.22	0.11	0.90	1.00
K_2O	0.37	0.07	0.37	0.37	0.39	0.36	0.48	0.45	0.44(10)	0.01	0.04	0.33	0.16
Total	99.21	99.67	98.65	98.85	98.50	98.58	99.27	99.19	98.96(21)	98.25	98.91	98.87	99.85
Mg/Al	0.52	–	0.50	0.51	0.51	0.51	0.32	0.34	0.31	6.00	3.45	0.25	0.07

Av. = Average.
n.a. = Not analyzed.
b.d. = Below detection.

values are ~3.1. This ratio is similar to the high-K KREEP (Jolliff 1998; Warren 2005) values from the Apollo 14 landing site (Table 5).

In a further comparison of SaU 169 regolith with other lunar soils, concentrations of main elements (Ca, Ti, Fe, Na, K, Mg, Al, Cr) and some trace elements (Sc, Sm, Eu, Hf, Ta, Th) were compared with Apollo and Luna regoliths and Calcalong Creek. Deviations of element ratios (sample/SaU 169 regolith) from unity were calculated and averaged for each regolith as a measure of similarity. SaU 169 regolith is most similar to Apollo 12 and 14 regoliths (25 and 21% mean deviation). Neither of the two sites provides a perfect match, however: Apollo 14 regolith is lower in Ti and more strongly enriched in incompatible elements; Apollo 12 regolith has higher Fe, Cr, and lower incompatible elements. Model mixtures of Apollo 12 and 14 soils (40:60, 17% mean deviation) or Apollo 14 regolith from which material of SaU 169 KREEP breccia clast composition is subtracted (–31% KREEP breccia clast, 17% mean deviation) yield still better matches. Differences remain for Fe, Ti, and Cr. After Apollo 12 and 14 soils, Calcalong Creek shows the next most similar composition (36% mean deviation).

In an attempt to quantitatively model the composition of SaU 169 regolith (for Si, Al, Fe, Mg, Ca, Na, K, Ti, Sc, Zr, Sm, Eu, Th) we used the following components: high-K KREEP (Warren 2005), anorthositic surface material (Korotev et al. 2003), average mare basalt (Warren 2005), norite 15455c, and troctolite 76535 (Taylor et al. 1991). The proportions of different components were determined by iteration of the following three steps: 1) the fraction of high-K KREEP is adjusted to obtain a minimum average deviation of Zr, Sm, Eu, and Th from measured values; 2) the basalt fraction is adjusted to obtain the measured Al concentration; and 3) the norite/troctolite relative proportion was adjusted to obtain the best fit for all elements (if applicable). Mixtures of ~36% high-K KREEP, 26% mare basalt, 26% norite, and 12% troctolite produce a composition closely resembling the SaU 169 regolith (5% mean deviation of all elements). A classical approach, using the three components high-K KREEP (36%), anorthosite (30%), and mare basalt (34%) yields a less well-fitting composition (8% mean deviation), which is low in Mg and high in Ca. All models show deficits of Na_2O and K_2O, possibly indicating the presence of a component rich in alkali feldspar. The bulk composition can more closely be modeled by adding such a feldspar component, but this was omitted here because we have no petrographic proof.

The similarities between SaU 169 regolith and other lunar soils and regoliths are particularly evident for the relations between FeO-TiO_2-Cr_2O_3 (closest to Apollo 14), Sm-Al_2O_3 (Fig. 10), Sm/Eu ratio, and total incompatible elements (e.g., Th). Relations between K and Th reveal, however, that the SaU 169 regolith has undepleted K/Th of 452 (Apollo 12: 435; Calcalong Creek: 466), while Apollo 14 soils (343), SaU 169 impact melt (137), and KREEP breccia clast (337) are depleted in K.

DISCUSSION

Shock History

Estimation of the shock grade that led to the shock-lithification of the regolith is difficult because shock grade indicators like the formation of shock melts are influenced by rock porosity (e.g., Kieffer 1976). Thus, much lower shock pressures may lead to increased melting in regoliths than in solid rocks on which the classification of Stöffler et al. (1991) is based. By combining the petrologic with radiometric and

Table 5. Chemical analysis of SaU 169 bulk regolith, KREEP breccia clast, and Apollo 14 KREEP rocks.

Method		SaU 169 bulk regolith	SaU 169 KREEP breccia clast	Apollo 14	SaU 169 impact-melt breccia	1σ error (%)[a]
		Breccia	Breccia	High-K KREEP	IMB	
OES	SiO_2	46.9[b]	46.86	50.3	45.15	0.9
OES	Al_2O_3	17.54	16.34	15.1	15.88	1.2
OES	FeO_{tot}	11.09	8.8	10.3	10.67	1.9
OES	MnO	0.14	0.12	0.14	0.14	2.2
OES	MgO	7.94	6.92	8.29	11.09	4.6
OES	CaO	11.72	10.6	9.79	10.16	1.9
OES	Na_2O	0.78	1.18	0.94	0.98	4.4
OES	K_2O	0.46	0.88	0.96	0.54	4.0
OES	TiO_2	2.49	1.47	2	2.21	3.1
OES	P_2O_5	0.42	0.76	1.60	1.14	7.0
OES	Sc	28	18	23	25	7.4
MS/OES	V	61	36	40	36	5.4
MS	Cr	1310	811	1200	992	4.4
MS	Co	19	12	25	31	7.6
MS	Ni	82	58		204	15
MS	Rb	10	20	22	13.7	10
MS/OES	Sr	214	230	200	359	4.6
MS/OES	Y	162.5	338	400	532	8.7
MS/OES	Zr	596	1397	1400	2835	6.9
MS	Nb	18	112	100	124	13
MS	Cs	0.4	0.9	1	0.8	6.4
MS/OES	Ba	593	1351	1300	1520	7.2
MS	La	52	113	110	170	4.1
MS	Ce	139	297	280	427	7.8
MS	Pr	17.1	35.6	37	57.5	10
MS	Nd	76.9	162	178	257	5.2
MS	Sm	21.9	44.9	48	70.15	5.0
MS	Eu	2.43	2.45	3.3	4.2	5.4
MS	Gd	25.3	50.4	58	86.4	17
MS	Tb	5.08	10.5	10	15.1	10
MS	Dy	30.7	63.9	65	94.2	9.2
MS	Ho	6.36	13.0	14	21.3	8.2
MS	Er	18.6	39.3	40	58.1	12
MS	Tm	2.72	5.96	5.7	9.13	11
MS	Yb	16.9	36	36	54.7	15
MS	Lu	2.53	5.24	5	7.64	7.9
MS	Hf	14.8	34.7	38	64.3	12
MS	Ta	2.14	4.16	5	7.1	25
MS	W	1.3	2.5	3	3.5	29
MS	Th	8.44	21.7	22	32.7	5.2
MS	U	2.27	5.83	6.1	8.6	5.6
	La/Yb	3.1	3.1	3.1	3.1	

[a]Standard deviation of measured divided by certified or recommended values.
[b]Microprobe value on regolith shock glass.
SaU 169 bulk regolith, KREEP clast, and impact-melt breccia are from Gnos et al. (2004).
IMB = impact-melt breccia.
Apollo 14 high-K KREEP from Warren (2005).
n.a. = Not analyzed.
Elements below detection: Cu <20, Zn <60, and Pb <10 ppm.

noble gas data (Gnos et al. 2004; Lorenzetti et al. 2005), a tentative correlation of events with age results (Table 1) was deduced: 1) The SaU 169 impact-melt breccia was excavated and brought to a regolith position at unknown depth ~2800 Myr ago, and 2) it is most likely that the older (stage II) regolith of SaU 169 became shock lithified ~200 Myr ago during an impact and attached to a fragment of the 3909 ± 13 Ma old Imbrium impact-melt breccia (Gnos et al. 2004). This impact brought the impact-melt breccia and attached older regolith into the younger regolith (stage III) position close to the surface because the younger regolith shows a solar-wind noble-gas component (Gnos et al. 2004;

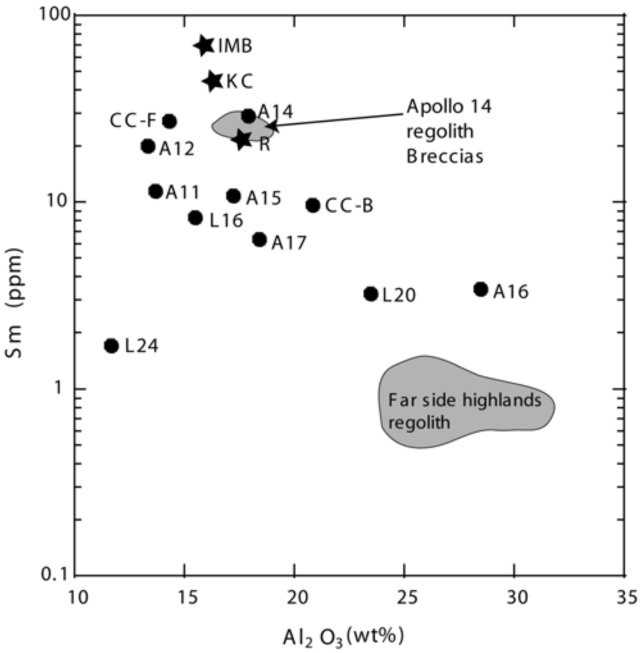

Fig. 10. Sm versus Al_2O_3 diagram, showing that the SaU 169 lithologies and more pronounced the SaU 169 regolith part are related to the Apollo 14 KREEP suite and soil and regolith breccias, but are different from other Apollo and Luna soil and regolith breccias and the lunar farside highland regolith. Star denotes subsamples of SaU 169. IMB = impact-melt breccia; KC = KREEP breccia clast; R = regolith; A = Apollo average soil and regolith breccia; L = Luna average soil and regolith breccia; CC-F = Calcalong Creek clast F; CC-B = Calcalong Creek bulk composition.

Lorenzetti et al. 2005). Moreover, the lithologic content of this younger regolith is different, containing impact-melt glass shards and beads, pyroxferroite-bearing basalts, a picrobasalt clast, and a pyroxferroite breakdown clast. A vesicle-rich flow-banded impact-melt glass separates it from the older regolith. The last recorded impact on the SaU 169 regolith is ~340,000 years ago which launched it into a solar system orbit (Gnos et al. 2004; Lorenzetti et al. 2005). As stage IV shock veins (Fig. 2) crosscut all lithologies, including the vesicle-rich flow-banded melt bordering the younger regolith (stage III), this event possibly corresponds to the impact that launched the rock to the Earth.

Regolith Components and Mineralogy

The wide range of Ti-poor to Ti-rich basalts and their variable mineral compositions (especially in the younger regolith) point to basalts derived from different sources. Most plagioclase clasts and plagioclase in rock fragments have compositions ranging from An_{74} to An_{94} and Or_0 to Or_2. Anorthite contents exceeding An_{94} are extremely rare. They were only observed in one gabbronorite clast (An_{96-97}) in the younger regolith (Fig. 5a) and in the KREEP breccia clast (An_{97}) in the older regolith (Fig. 2). This points to a limited contribution of anorthositic highland rocks. The low Fe contents in plagioclase indicate that all analyzed larger mineral clasts have a plutonic origin (Papike et al. 1991). (Papike et al. 1991). Based on a Th-FeO classification (Korotev et al. 2003), the SaU 169 regolith appears as a ternary mixture of KREEP material, mare basalts, and feldspathic material. However, the limited presence of anorthositic highland rocks clasts and the result of a whole-rock mixing model rather indicates a ternary mixture of mare basalts, KREEP, and Mg-suite rocks (Zeigler et al. 2006), which is consistent with a high abundance of relatively sodic feldspars in the regolith matrix.

Magnesium-rich olivine (Fo_{84}) as in SaU 169 was also found among the Apollo 12 and 14 highland samples by Warren (1993). Forsterite-rich clasts in regolith breccia have only been reported from the Apollo 17 landing site, and likely are derived from Serenitatis (Ryder et al. 1997). The presence of dunite (>90 vol% forsterite) xenoliths in lunar meteorite Dhofar (Dho) 310 (Demidova et al. 2003), however, suggests that such material may be more widespread. Even more exceptional is the large fayalite clast (Fig. 7), which is apparently derived from a strongly evolved magmatic rock. Fayalitic olivine (Fo_{12}) of similar composition as in the SaU 169 regolith was reported from Dho 287A (mare basalt portion) in the late-stage mesostasis part (Fo_{0-15}; Anand et al. 2003), from MET 01-210 (Patchen et al. 2005), and recently in the polymict regolith breccia NWA 3136 (Kuehner et al. 2005).

Ferroaugite-fayalite-quartz-bearing volcanic rocks are known in terrestrial peralkaline and tholeiitic suites (e.g., Scaillet and MacDonald 2001). In a compilation on silicate liquid immiscibility, Roedder (1979) described the close association of Fe-rich basaltic with potassic granitic melt in lunar samples. In our clast 11 (Fig. 4), closely associated ilmenite-fayalite seems to coexist with ferroaugite. The interstitial phase is silica glass. Although alkali feldspar is also a characteristic late-crystallizing phase in association with this assemblage, it was not observed in the small fragment. This could indicate that the assemblage represents a break-down assemblage of pyroxferroite, as proposed by Patchen et al. (2005).

Based on criteria described by Delano (1986) to distinguish volcanic glass from impact-melt glass, all analyzed glass fragments in the younger SaU 169 regolith are impact-melt glasses. The impact-glass data corroborate the noble-gas data (Gnos et al. 2004; Lorenzetti et al. 2005), which showed that the younger regolith represents the top few tens of centimeters of a lunar soil at the impact site from which the meteorite was launched into space.

Rock Chemistry

The REE pattern and the bulk chemical composition of the average regolith fall between the compositional fields of

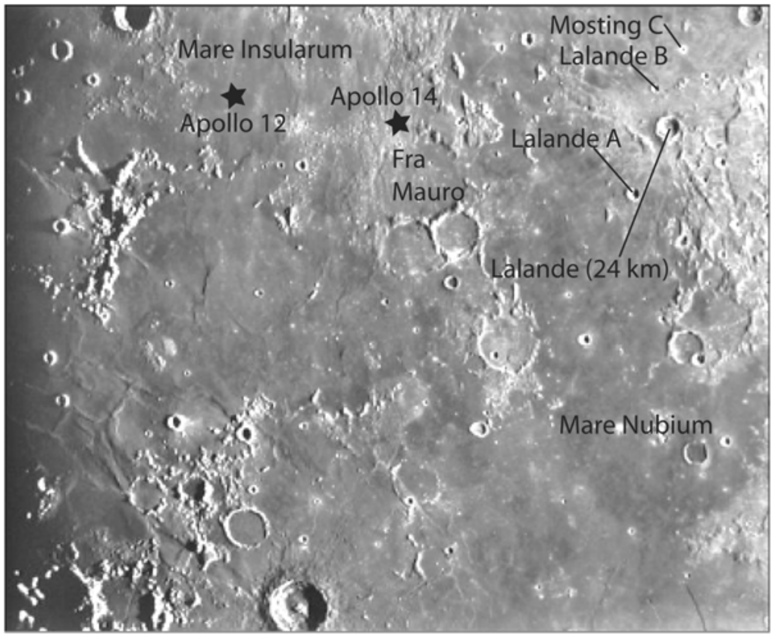

Fig. 11. Photograph of the Apollo 14 and 12 landing region (www.lunarrepublic.com/atlas/index.shtml) showing the proposed source region for the SaU 169 meteorite. Because the Lalande impact is located in the southeast of the lower corner of Mare Insularum, this supports the work by Gnos et al. (2004) proposing that the SaU 169 impact-melt breccia (oldest part of SaU 169) was excavated to a regolith position (regolith stage II in Fig. 2) by the Lalande impact at ~2800 Ma.

Apollo 14 and Apollo 12 soils and regolith breccias. Furthermore, the KREEP breccia clast REE content is very similar to the Apollo 14 KREEP breccias (Warren and Wasson 1979). Additionally, the Apollo 12 soil has 1.7 ppm U and 6.4 ppm Th, while the Apollo 14 soil has 1.5 ppm U and 6.7 ppm Th (McKay et al. 1991). These values are close to SaU 169 average regolith containing 2.27 ppm U and 8.44 ppm Th (Table 5). This indicates source proximity of the SaU 169 regolith to both Apollo 12 and 14 landing sites, like the Lalande crater region proposed by Gnos et al. (2004) on the basis of age results and regional Th-Fe-Ti-K concentrations (Gillis et al. 2004; Haskin et al. 2000; Lawrence et al. 1999).

The REE content of the SaU 169 KREEP breccia clast is very similar to the composition of the Apollo 14 high-K KREEP lithology, indicating that it is probably derived from the same region. This is also reflected in the total REE content of 879 ppm of the SaU 169 KREEP breccia clast, which is close to the 890 ppm measured in Apollo 14 high-K KREEP (Warren 2005). Normalized REE data clearly show that the SaU 169 KREEP breccia clast and the SaU 169 bulk regolith are different from the ultraKREEPy impact-melt rocks from Apollo 14 and 16 (Jolliff 1998). In comparison with data compiled by Korotev (1997) and Cahill et al. (2004), the Sc content and the Sm-Al_2O_3 concentrations (Fig. 10) show that the SaU 169 average regolith is most similar to the Apollo 14 KREEP suite and regolith breccias, but is different from other Apollo landing sites and the lunar farside highland regolith. The Sc content in the bulk regolith is slightly higher than that of the Apollo 14 high-K KREEP (23 ppm), indicating a larger proportion of mare basalt (Korotev 1991) than observed at the Apollo 14 site. Most basalt clasts have TiO_2 contents in the range of Ti-poor basalts (four) and medium-Ti basalts (three), indicating strong contribution of mare basalts similar to those observed at Apollo 12, Luna 24, and Apollo 14 sites (Le Bas 2001; Papike et al. 1991). This again supports proximity of the SaU 169 regolith source to Apollo 12 and 14 landing sites. Only two Ti-rich basalts were detected, indicating a small contribution of mare basalts from other sources.

Models for the composition of the SaU 169 regolith produce a closer match when mixtures of high-K KREEP, mare basalt, norite, and troctolite are used as compared with high-K KREEP, mare basalt, and anorthosite. This is consistent with the near-absence of anorthositic fragments. The applied model compositions are low in Na and K, indicating the possible presence of an additional component enriched in alkalis.

The variable BSE colors of the flow-banded shock melt are indicative of assimilated clast compositions. Light-colored bands most likely resulted from melting mineral or rock clasts with high FeO contents, and the dark bands result from melting Al_2O_3-rich clasts, like plagioclase (Table 4). Gray portions are interpreted as a homogenized mixture of molten clasts from the regolith stage III. Its composition therefore is interpreted as representing the average bulk composition of the younger stage III regolith and appears to be similarly KREEP-enriched as the bulk regolith composition listed in Table 5.

Comparison with KREEPy Lunar Meteorites

Although Korotev (2005) proposed that the impact-melt breccia of the SaU 169 represents a separate group of lunar meteorites that is different from other known lunar meteorites due to its very high concentration of Th and incompatible elements, the SaU 169 regolith material is comparable in composition to some KREEP clasts from lunar meteorites. Among the other lunar meteorites, Calcalong Creek (Hill and Boynton 2003), Yamato- (Y-) 983885 (Karouji et al. 2006), and Dho 925/961 (Korotev et al. 2006) are reported to be KREEPy. The Calcalong Creek Na_2O, K_2O, Th, U, and total REE concentrations (Hill and Boynton 2003) are well below those of SaU 169, but one KREEP clast (clast F) in Calcalong Creek is in the range of SaU 169 regolith. However, the elevated K/Th of 596 in the Calcalong Creek clast indicates an admixture of alkali-enriched KREEP, complementary to depleted Apollo 14 soil (343), SaU 169 IMB (137), and KREEP breccia clast (337), while SaU 169 regolith has a pristine KREEP K/Th ratio (452).

SaU 169 is clearly different from other lunar meteorites found in the south of Oman, (Dho 025, 262, 081) which sample highland compositions and probably are derived from the lunar farside (Cahill et al. 2004; Cohen et al. 2004). Although olivine with nearly pure fayalitic composition was found in the SaU 169 regolith, NWA 3136 (Korotev and Irving 2005), and Dho 287A (Anand et al. 2003), source-crater pairing is unlikely because of the much higher KREEP component in the SaU 169 regolith.

Regolith Origin on the Moon

Based on a combination of age and chemical data obtained on SaU 169, the history of the rock has been constrained to the area surrounding the Imbrium basin (Gnos et al. 2004). If these data are combined with the noble gas data of Lorenzetti et al. (2005) and the data presented in this study, the original dataset can be refined.

The noble gas data indicate that the shock-compaction of the older regolith (stage II) occurred at a depth of a few meters below the surface at ~200 Ma (Gnos et al. 2004). Thus the older regolith probably represents a sample of a relatively deep-seated regolith from the Lalande crater area. The younger regolith (stage III in Fig. 2), which is compositionally distinct from the older regolith, contains a solar-wind noble-gas component (Gnos et al. 2004; Lorenzetti et al. 2005), which means that components of this regolith were exposed at the topmost surface of the Moon.

A source area for SaU 169 in the region of the Apollo 14 and 12 landing sites is likely because:

1. The regolith bulk chemistry, including REEs, is close to that of the soil and regolith breccia of Apollo 12 and 14 landing sites (Haskin and Warren 1991), but with some differences.
2. The bulk chemistry and the REE content of the KREEP breccia clast is very similar to that of the Apollo 14 ITE-rich high-K KREEP (Jolliff 1998; Warren 2005).
3. The Sm versus Al_2O_3 (Fig. 10) data show that the regolith breccia plot in the field of the Apollo 14 regolith breccias (Cahill et al. 2004; Warren and Wasson 1980).
4. Most basalt clasts have TiO_2 contents in the range of Ti-poor basalts (four) and medium-Ti basalts (three), indicating a strong contribution from mare basalts similar to those from the Apollo 12, Luna 24, and Apollo 14 (Le Bas 2001; Papike et al. 1991). Scandium values support this interpretation.
5. The Fe-Ti-Th-K ratios derived from remote-sensing data (Gillis et al. 2004; Haskin et al. 2000; Lawrence et al. 1999) are consistent with the regolith bulk chemistry for this area;
6. The Th and U concentrations in returned Apollo 12 and 14 soils are close to those of the SaU 169 average regolith.
7. KREEP basalts, which are common at the Apollo 15 landing site located on the eastern rim of the Imbrium basin near Aristillus (but not at the Apollo 12 and 14 sites) are not observed in the SaU 169 regolith.
8. Fe-rich basaltic rocks like our basalt 11 (Fig. 4) are common in the Apollo 12 collection (e.g., Roedder 1979).

The absence of a depletion of K relative to Th, as observed in the SaU 169 impact-melt breccia, SaU 169 regolith KREEP breccia clast, and also in Apollo 14 soils, indicates that impact-melt breccias such as the main lithology of SaU 169 represent only a minor fraction of the regolith at the ejection site. The petrological and chemical data and the proximity of the proposed Lalande crater area to the Apollo 12 and 14 landing sites (Fig. 11) are consistent with the work by Gnos et al. (2004), which proposed that the Lalande impact crater is the most plausible site where the SaU 169 impact-melt breccia was excavated and brought to a regolith position ~2800 Myr ago.

CONCLUSIONS

SaU 169 is a unique lunar meteorite sampling mainly Procellarum KREEP terrane-derived material. Its regolith comprises rock and mineral fragments embedded in a fine ground mass. Only one highland anorthosite rock fragment was found. The SaU 169 regolith and the KREEP breccia clast have chemical compositions typical for KREEP rocks and are similar to soils and regolith breccias sampled at the Apollo 14 and Apollo 12 landing sites. Relations between Sm-Al_2O_3 (Fig. 10), FeO-Cr_2O_3-TiO_2, K-Th, and the Sm/Eu value (Table 5) are also similar to the Apollo 14 KREEP suite and regolith breccia. The ferroaugite-fayalite-silica clast and the large magmatic fayalite clast probably represent highly evolved magmas as studied in Apollo 12 material

(Roedder 1979). The chemical composition of the SaU 169 regolith is clearly different from that of other lunar meteorites, except for one KREEP clast (clast F) described from the Calcalong Creek lunar meteorite (Hill and Boynton 2003).

Acknowledgments–Dr. Hilal Al Azri, Ministry of Commerce and Industry, Muscat, and Akram Al Muraza, Khalid Musallam Al Rawas, and Sami Al Zubaidi, Ministry of Commerce and Industry, Salalah, are thanked for their support during the project. This study was supported by the Swiss National Science Foundation grants 2100-064929, 200020-107681 and microprobe credits 21-26579.89 and 200021-103479/1. J. Day, P. Warren, and R. Korotev are thanked for the constructive and detailed reviews.

Editorial Handling—Dr. Randy Korotev

REFERENCES

Anand M., Taylor L. A., Misra K. C., Demidova S., and Nazarov M. A. 2003. KREEPy lunar meteorite Dhofar 287A: A new lunar mare basalt. *Meteoritics & Planetary Science* 38:485–499.

Anders E. and Gravesse N. 1989. Abundances of the elements—Meteoritic and solar. *Geochimica et Cosmochimica Acta* 53:197–214.

Cahill J. T., Floss C., Anand M., Taylor L. A., Nazarov M. A., and Cohen B. A. 2004. Petrogenesis of lunar highlands meteorite: Dhofar 081, Dar al Gani 262, and Dar al Gani 400. *Meteoritics & Planetary Science* 39:503–529.

Cohen B. A., James O. B., Taylor L. A., Nazarov M. A., and Barsukova L. D. 2004. Lunar highland meteorite Dhofar 026 and Apollo sample 15418: Two strongly shocked, partially melted, granulitic breccias. *Meteoritics & Planetary Science* 39:1419–1447.

Delano J. W. 1986. Pristine lunar glasses: Criteria, data, and implications. Proceedings, 16th Lunar and Planetary Science Conference. pp. D201–D213.

Demidova S., Nazarov M. A., Kurat G., Brandstätter F., and Ntaflos T. 2003. Lunar meteorite Dhofar 310: A polymict breccia with deep-seated lunar crustal material (abstract). *Meteoritics & Planetary Science* 38:A30.

Gillis J. J., Jolliff B. L., and Korotev R. L. 2004. Lunar surface geochemistry: Global concentrations of Th, K, and FeO as derived from lunar prospector and Clementine data. *Geochimica et Cosmochimica Acta* 68:3791–3805.

Gnos E., Hofmann B., Al-Kathiri A., Lorenzetti S., Eugster O., Whitehouse M. J., Villa I. M., Jull A. J. T., Eikenberg J., Spettel B., Krähenbühl U., Franchi I. A., and Greenwood R. C. 2004. Pinpointing the source of a lunar meteorite: Implications for the evolution of the moon. *Science* 305:657–659.

Haskin L. A. and Warren P. 1991. Lunar chemistry. In *Lunar source book: A user's guide to the Moon*, edited by Heiken G. H., Vaniman D. T., and French B. M. Cambridge: Cambridge University Press. pp. 357–474.

Haskin L. A., Gillis J. J., Korotev R. L., and Jolliff B. L. 2000. The material of the lunar Procellarum KREEP terrain: A synthesis of data from geomorphological mapping, remote sensing, and sample analysis. *Journal of Geophysical Research* 105:20,403–20,415.

Hill D. H. and Boynton W. V. 2003. Chemistry of the Calcalong Creek lunar meteorite and its relationship to lunar terranes. *Meteoritics & Planetary Science* 38:595–626.

Jolliff B. L. 1998. Large-scale separation of K-frac and KREEP-frac in the source regions of Apollo impact-melt breccias, and a revised estimate of the KREEP composition. *International Geology Review* 40:916–935.

Kieffer S. W. 1976. Shock processes in porous quartzite: Transmission electron microscope observations and theory. *Contributions to Mineralogy and Petrology* 59:41–93.

Korotev R. 1997. Some things we can infer about the Moon from the composition of the Apollo 16 regolith. *Meteoritics & Planetary Science* 32:447–478.

Korotev R. L., Jolliff B. L., Zeigler R. A., Gillis J. J., and Haskin L. A. 2003. Feldspathic lunar meteorites and their implications for compositional remote sensing of the lunar surface and the composition of the lunar crust. *Geochimimica et Cosmochimica Acta* 67:4895–4923.

Korotev R. L. 2005. Lunar geochemistry as told by lunar meteorites. *Chemie der Erde* 65:297–346.

Korotev R. L. and Irving M. A. 2005. Compositions of three lunar meteorites: Meteorite Hills 01210, Northeast Africa 001, and Northwest Africa 3136 (abstract #1220). 36th Lunar and Planetary Science Conference. CD-ROM.

Kuehner S. M., Irving M. A., Rumble D. I., Hupé A. C., and Hupé G. M. 2005. Mineralogy and petrology of lunar meteorite NWA 3136: A glass-welded mare regolith of mixed heritage (abstract #1228). 36th Lunar and Planetary Science Conference. CD-ROM.

Lawrence D. J., Feldman W. C., Barraclough B. L., Binder A. B., Elphic R. C., Maurice S., Miller M. C., and Prettyman T. H. 1999. High-resolution measurements of absolute thorium abundances on the lunar surface. *Geophysical Research Letters* 26:2681–2684.

Le Bas M. J. 2001. Report of the working party on the classification of the lunar igneous rocks. *Meteoritics & Planetary Science* 36: 1183–1188.

Lorenzetti S., Busemann H., and Eugster O. 2005. Regolith history of lunar meteorites. *Meteoritics & Planetary Science* 40:315–327.

McKay D. S., Heiken G., Basu A., Blanford G., Simon S., Reedy R., French B. M., and Papike J. J. 1991. The lunar regolith. In *Lunar source book: A user's guide to the Moon*, edited by Heiken G. H., Vaniman D. T., and French B. M. Cambridge: Cambridge University Press. pp. 285–356.

Morimoto N., Fabries J., Ferguson A. K., Ginzburg I. V., Ross M., Seifert F. A., Zussman J., Aoki K., and Gottardi G. 1988. Nomenclature of pyroxenes. *Schweizerische Mineralogische und Petrographische Mitteilungen* 68:95–111.

Neal C. R. and Taylor L. A. 1992. Petrogenesis of mare basalts: A record of lunar volcanism. *Geochimica et Cosmochimica Acta* 56:2177–2211.

Papike J. J., Taylor L. A., and Simon S. B. 1991. Lunar minerals. In *The evolution of the igneous rocks*, edited by Yoder H. S. Princeton: Princeton University Press. pp. 15–58.

Papike J. J. 1998. *Planetary materials*. Washington, D.C.: The Mineralogical Society of America. pp. 1–893.

Papike J. J. 1998. Comparative planetary mineralogy: Chemistry of melt-derived pyroxene, feldspar, and olivine. In *Planetary materials*, edited by Papike J. J. Washington, D.C.: Mineralogical Society of America. pp. 7-01–7-11.

Papike J. J., Karner J. M., and Shearer C. K. 2003. Determination of planetary basalt parentage: A simple technique using the electron microprobe. *American Mineralogist* 88:496–472.

Patchen A. D., Taylor L. A., and Day M. D. 2005. Mineralogy and petrography of lunar mare regolith breccia meteorite MET

01-210 (abstract #1411). 36th Lunar and Planetary Science Conference. CD-ROM.

Roedder E. 1979. Silicate liquid immiscibility in magmas. In *Lunar source book: A user's guide to the Moon*, edited by Heiken G. H., Vaniman D. T., and French B. M. Cambridge: Cambridge University Press. pp. 121–181.

Scaillet B. and MacDonald R. 2001. Phase relations of peralkaline silicic magmas and petrogenetic implications. *Journal of Petrology* 42:825–845.

Taylor G. J., Warren P., Ryder G., Delano J., Peters C., and Lofgren G. 1991. Lunar rocks. In *Lunar source book: A user's guide to the Moon*, edited by Heiken G. H., Vaniman D. T., and French B. M. Cambridge: Cambridge University Press. pp. 183–284.

Warren P. H. and Wasson J. T. 1979. The origin of KREEP. *Reviews of Geophysics and Space Physics* 17:73–88.

Warren P. H. and Wasson J. T. 1980. Further foraging for pristine nonmare rocks: Correlations between geochemistry and longitude. Proceedings, 11th Lunar and Planetary Science Conference. pp. 431–470.

Warren P. 2005. The Moon. In *Meteorites, comets, and planets*, edited by Davis A. M. Treatise on Geochemistry, vol. 1. Amsterdam: Elsevier. pp. 559–599.

Zeigler R. A., Korotev R. L., and Jolliff B. L. 2006. Geochemistry and petrography of high-Th, mafic impact-melt breccia from Apollo 12 and Sayh al Uhaymir 169 (abstract #2366). 37th Lunar and Planetary Science Conference. CD-ROM.